UV-induced formation of the thymine-thymine pyrimidine (6-4) pyrimidone photoproduct - a DFT study of the oxetane intermediate ring opening

Vanessa Labet, Nelly Lidia Jorge, Christophe Morell, Thierry Douki, Jean Cadet, André Grand, Leif A. Eriksson

Photochemical & Photobiological Sciences

RSC Publishing

PAPER

View Article Online
View Journal

Cite this: DOI: 10.1039/c3pp50069a

UV-induced formation of the thymine–thymine pyrimidine (6-4) pyrimidone photoproduct – a DFT study of the oxetane intermediate ring opening†

Vanessa Labet,*[a] Nelly Jorge,[b] Christophe Morell,[c] Thierry Douki,[d] André Grand,[d] Jean Cadet[d,e] and Leif A. Eriksson[f]

The mechanism by which the hypothetical oxetane/azetidine intermediate formed during the photochemical process leading to pyrimidine (6-4) pyrimidone photoproducts when DNA is submitted to UV radiation opens is investigated computationally by DFT using a 5′-TT-3′ dinucleoside monophosphate as a structural model. First, the feasibility of an intramolecular mechanism involving one proton transfer inducing opening of the oxetane ring is examined. It results in a very high Gibbs energy of activation (+166 kJ mol^{-1}) and quite a low Gibbs energy of reaction (–35 kJ mol^{-1}). The protonation state of the phosphate group is shown to have little effect while the bulk effect of an aqueous environment modeled by the Polarizable Continuum Model method lowers slightly the activation barrier (by about 10–20 kJ mol^{-1}), not enough to explain the fact that the oxetane intermediate is not observed experimentally. Then the catalytic effect of water molecules on the reaction pathway is studied by including either 1 or 2 assisting water molecules in the chemical system. The resulting activation barrier is considerably lowered and in the most favorable situation – a phosphate group deprotonated and 2 assisting water molecules – the Gibbs energy activation is as low as +44 kJ mol^{-1} and the Gibbs energy of reaction is quite favorable: –79 kJ mol^{-1}, suggesting that in biological systems the oxetane ring opening process proceeds with explicit intervention of water molecules from the environment.

Received 27th February 2013,
Accepted 17th June 2013

DOI: 10.1039/c3pp50069a

www.rsc.org/pps

1. Introduction

Solar UV radiation is a major mutagenic agent responsible for the induction of most skin cancers.[1] These deleterious properties are explained by the efficient absorption of UV-B photons (290–320 nm) by DNA. The resulting excitation leads to the formation of photo-cycloaddition products between adjacent pyrimidine bases (thymine, T and/or cytosine, C).[2] The biological role of these events is unambiguously shown by the predominance of mutations at bipyrimidine sites in skin tumors.[3,4]

Two types of photoproducts can be produced at each of the four bipyrimidine dinucleotides, as illustrated in Fig. 1 in the case of a 5′-TT-3′ bipyrimidine site. In the first type, [2 + 2] cycloaddition between the two C5–C6 double bonds of the bases results in the formation of cyclobutane pyrimidine dimers (CPDs). The second type of lesion is generally thought to involve Paternó–Bücchi [2 + 2] cycloaddition of the C5–C6 double bond of the 5′-end base to either the C4═O bond of a 3′-end thymine or the exocyclic imino group of a tautomeric form of a 3′-end cytosine. This latter photoreaction is proposed to lead to unstable cyclic intermediates that exhibit oxetane and azetidine structures, respectively, as sketched in Fig. 1B in the case of a 5′-TT-3′ bipyrimidine site. If the formation of cyclic intermediates has never been observed for thymine and cytosine, stable oxetanes arising for the cycloaddition of thymine and aromatic ketones were isolated.[5,6] And a thietane derivative, the cyclic intermediate involved in the formation of the second type of photodamage between thymine and 4-thiothymine, could also be isolated and extensively characterized by spectroscopic methods.[7] In addition, recent time-resolved measurements showed that the formation of these

[a]UPMC Univ Paris 06, UMR 7075, LADIR, F-75005 Paris, France. E-mail: vanessa.labet@upmc.fr
[b]Laboratorio de Investigaciones en Tecnologia del Medio Ambiante, FACENA-UNNE, Av. Libertad 5640, 3400 Corrientes, Argentina
[c]Univ Lyon 1, ISA, UMR 5280, 5 rue de la Doua, F-69100 Villeurbanne, France
[d]CEA Grenoble – INAC/SCIB/LAN (UMR-E n°3 CEA-UJF), CEA-Grenoble, 17, rue des Martyrs, F-38054 Grenoble Cedex 9, France
[e]Univ Sherbrooke, Fac Med & Sci Sante, Dept Med Nucl & Radiobiol, Sherbrooke, PQ J1H 5N4, Canada
[f]Department of Chemistry and Molecular Biology, University of Gothenburg, 412 96 Göteborg, Sweden

†Electronic supplementary information (ESI) available: Full citation for ref. 23; Fig. S1: Product distribution of photoproducts in UVB exposed DNA. See DOI: 10.1039/c3pp50069a

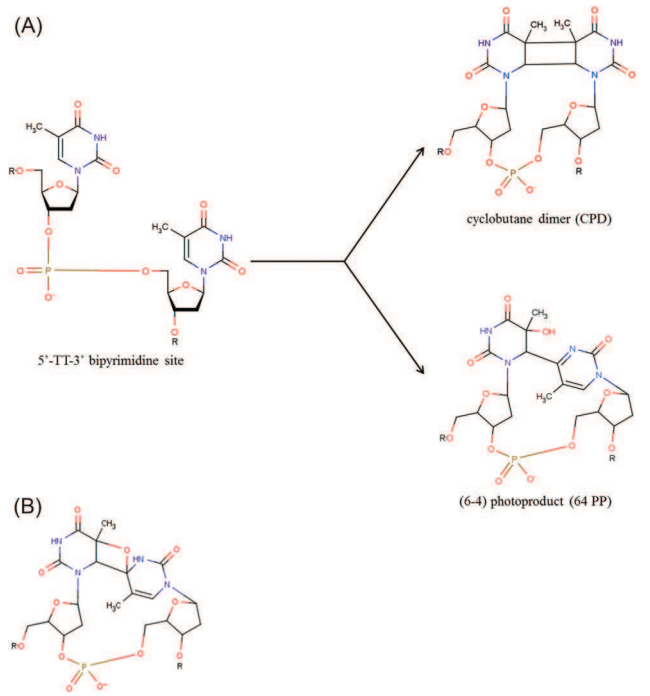

Fig. 1 (A) Chemical structure of the main UVB-induced dimeric photoadducts produced at a 5′-TT-3′ bipyrimidine site. (B) Hypothetical oxetane intermediate in the formation of 6-4PP.

photoproducts in double-stranded DNA is much slower than that of CPDs, likely because of the formation of the cyclic intermediates.[8] Rearrangement of the latter yields stable photoproducts exhibiting a saturated pyrimidine moiety on the 5′-end covalently linked to a pyrimidone moiety on the 3′-end. This class of photodamage is thus referred to as pyrimidine (6-4) pyrimidone photoproducts (6-4PPs). They are believed to arise from a singlet excited state. Indeed, experiments involving triplet energy transfer photosensitization led to the sole production of CPDs.[9–11] A number of reactivity differences between the two pyrimidine bases have been inferred based on the yield of formation of the two kinds of dimeric photoproducts at each bipyrimidic site (see Fig. S1 in the ESI†):

(1) The CPDs are produced more efficiently than the related (6-4) photoproducts. This is particularly true when a thymine is at the 3′-end of the bipyrimidine site;
(2) thymines appear to be more reactive than cytosine toward the formation of dimeric photoproducts; and
(3) there is a sequence dependence since photoproducts are not produced in the same yield at 5′-TC-3′ and 5′-CT-3′ sites.[12–15]

Some mechanistic and energetic information about CPD and 6-4PP formation has been afforded by computational studies. For example, the higher reactivity of thymine *versus* cytosine has been proposed to originate from the more favorable excited-state energy barriers, and a smaller energy gap between the ground state (g.s.) and the relevant excited state at the g.s. transition state structure.[16–18] In addition, recent studies suggest that if the formation of CPDs involves ππ* excitons, that of the oxetane/azetidine intermediates in the formation of 6-4PPs involves charge transfer excited states and therefore does not proceed *via* a Paternó–Bücchi cycloaddition as was thought originally.[19–21] Nonetheless, quite interestingly, a qualitative theoretical study based on the use of conceptual DFT reactivity indices for both the ground state and the 1st excited state (ππ* exciton) proposed an explanation for the regioselectivity observed between CPDs and 6-4PPs by considering that the oxetane/azetidine intermediate in the formation of 6-4PP photoproducts results from a Paternó–Bücchi cycloaddition. Indeed, in the corresponding excited state, thymines are characterized by the O4′ oxygen participating in the [2 + 2] cycloaddition being more electrophilic than nucleophilic, and therefore react unfavorably with the electrophilic carbon C5 of its partner. In contrast, the equivalent nitrogen in the imino form of cytosine is more nucleophilic than electrophilic and can react in a favorable way with the electrophilic carbon C5 of its partner.[22]

Thus, the mechanism by which the oxetane/azetidine intermediate is formed is still subject to debate. In this work we propose to focus on the second step of the formation of the 6-4PP photoproducts, *i.e.* the mechanism by which the 4-membered ring of the oxetane/azetidine intermediate opens. The objective is to gain insight into the reasons why the cyclic intermediate is generally not observed. To the best of our knowledge, this is the first time that this question has been investigated computationally. In particular, the influence of the protonation state of DNA phosphate groups as well as that of water molecules in the environment is examined.

2. Theoretical model

It was decided to focus on the formation of the 6-4PP produced at thymine–thymine bipyrimidic sites once the oxetane intermediate has been formed. To model the chemical system, the corresponding dinucleoside monophosphate was used. As such, the reaction studied in this work is shown in Fig. 2 where the atom labeling used in the following is also indicated. Note that in Fig. 2 the phosphate group has been sketched as deprotonated. The same reaction has also been studied with a protonated phosphate group.

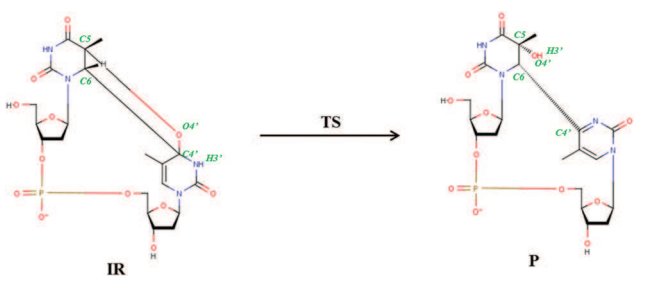

Fig. 2 Reaction mechanism studied in this work.

As sketched in Fig. 2, the reaction involves transfer of the H3′ proton from nitrogen N3′ to oxygen O4′, and concomitantly, breaking of the oxetane ring. Contrary to the formation of the oxetane intermediate, it is expected that this step takes place in the ground state. Therefore, the reaction mechanism was explored in the ground state only.

3. Computational details

3.1. General procedure

The geometries of the stationary points corresponding to the proposed mechanism (see Fig. 2) were optimized in their ground state using the B3LYP hybrid functional and the 6-31G (d,p) double-zeta basis set. Frequency calculations were performed at the same level of theory within the harmonic approximation, in order to check that IR and P corresponded to minima of the ground state potential energy surface (no imaginary frequency), while TS was indeed a 1st order saddle point (exactly one imaginary frequency). The vibrational analysis was also used to extract thermodynamic quantities of activation and reaction for the elementary step. From TS, intrinsic reaction coordinate calculations (IRC) were performed to ensure that the transition state connects the oxetane intermediate IR and the (6-4) photoproduct P.

All calculations were performed using the Gaussian 03 and Gaussian 09 packages.[23]

3.2. Evaluation of the basis set effect

Energy calculations with the 6-31++G(d,p) basis set were performed on the structures of IR, TS and P optimized with the 6-31G(d,p) basis set in order to evaluate the effect of adding diffuse functions in the basis set.

3.3. Evaluation of the solvent effect

In order to have a good estimation of the solvent effect at reasonable computational cost, the bulk effect of an aqueous environment was studied by performing single point energy calculations on the optimized structures for IR, TS and P including a polarized continuum model in the integral equation formalism (PCM)[24–26] with a dielectric constant of ε = 78.39. The cavity for the solute was built using the United Atom Topologic Model applied on the atomic radii of the UFF force field, with an average area of 0.2 Å^2 for the tesserae generated on each sphere. The default cavity was modified by adding individual spheres to all hydrogen atoms linked to nitrogen and oxygen atoms, using the keyword SPHEREONH. Enthalpies and Gibbs energies of activation and reaction in aqueous solution were then evaluated by adding the solvation energies to the corresponding thermochemical quantities obtained in a vacuum from the frequency calculations mentioned above (Section 3.1).

In addition, the possibility to form hydrogen bonds between the biological solute and water molecules from the solvent was investigated by including discrete H_2O molecules – either one or two – in the system studied computationally. Stationary points were re-optimized accordingly (IR-H_2O, TS-H_2O and P-H_2O with 1 additional water molecule and IR-2H_2O, TS-2H_2O and P-2H_2O with 2 additional water molecules). The same methodology as described above was followed to extract thermochemical data and evaluate the bulk effect of an aqueous environment.

4. Results and discussion

A minimum of the ground state potential energy surface of the reaction, corresponding to the IR intermediate, was identified for both a protonated and a deprotonated phosphate group. In both cases it shows a real oxetane structure with a four-membered ring involving four completely formed C–C and C–O single bonds, as suggested by the following bond lengths: $l_{C5–C6}$ = 1.54 Å, $l_{C6–C4'}$ = 1.59 Å, $l_{C4'–O4'}$ = 1.46 Å and $l_{O4'–C5}$ = 1.46 Å. Thus the oxetane intermediate corresponds to a stable structure from an electronic point of view. In the case of a protonated phosphate group, IR shows a ZPE-corrected energy E at T = 298 K and P = 1 atm about 160 kJ mol^{-1} higher than that of the corresponding dinucleoside monophosphate. This can be compared to the energy of the corresponding CPD, studied by Durbeej and Eriksson,[16] which is about 85 kJ mol^{-1} higher in energy than two thymines. It can thus be concluded that the oxetane intermediate is far less stable than the corresponding cyclobutane.

Once the oxetane intermediate has been formed on the ground state potential energy surface, the four-membered ring has to be broken so that the corresponding 6-4PP be formed. As can be seen in Fig. 2, this involves the transfer of hydrogen H3′ from nitrogen N3′ to oxygen O4′ that in turn induces the ring opening. Two mechanisms were studied for this transfer: either directly (intramolecular hydrogen transfer) or with the assistance of water molecule(s) from the environment.

4.1. Intramolecular H transfer

4.1.1 Influence of the protonation state of the phosphate group. A transition state TS was optimized, directly linking the oxetane intermediate IR to the product P on the ground state potential energy surface. Its geometry is shown in Fig. 3 along with those of IR and P. Relevant distances particularly modified during the reaction are indicated in Table 1 for the three stationary points of the elementary step, in the case of a protonated phosphate group as well as in the case of a deprotonated one. The corresponding relative energies are reported in Table 2.

For both protonation states of the phosphate group, the transition state structure displays an N3′–H3′ bond distance only slightly elongated (from 1.01 Å to either 1.04 Å (deprotonated) or 1.06 Å (protonated)) with respect to the oxetane structure, while the C4′–O4′ distance has evolved from 1.46–1.47 Å to 2.30–2.33 Å. Thus, TS is an early transition state for the N3′–H3′ bond breaking but a quite late transition state for the oxetane ring opening. Therefore, this elementary step involves an asynchronous concerted mechanism, with the

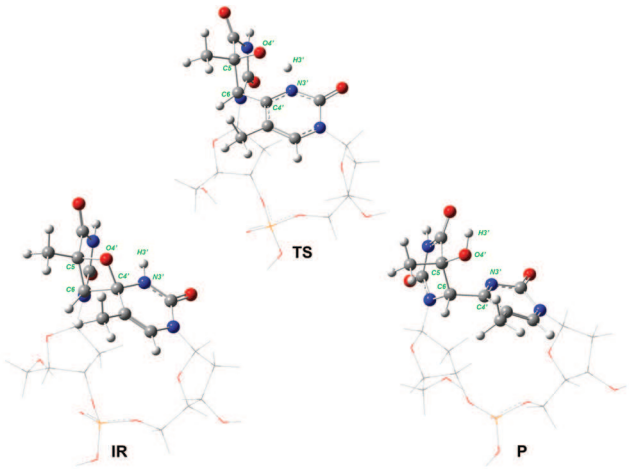

Fig. 3 Optimized geometries of IR, TS and P in the case of a protonated phosphate group.

Table 1 Evolution of key interatomic distances (in Å) during the IR–TS–P elementary step, for protonated and deprotonated states of the phosphate group

		IR	TS	P
Protonated	$l_{N3'-H3'}$	1.01	1.06	3.88
	$l_{O4'-H3'}$	2.60	1.73	0.98
	$l_{C4'-O4'}$	1.46	2.30	2.78
Deprotonated	$l_{N3'-H3'}$	1.01	1.04	3.87
	$l_{O4'-H3'}$	2.61	1.93	0.98
	$l_{C4'-O4'}$	1.47	2.33	2.80

Table 2 Evolution of the ZPE-uncorrected energy E_0, ZPE-corrected energy E, enthalpy H and Gibbs energy G (in kJ mol^{-1}) at T = 298 K and P = 1 atm in a vacuum during the IR–TS–P elementary step for protonated and deprotonated states of the phosphate group. ZPE-uncorrected energies E_0 resulting from single point computations performed with the 6-31++G(d,p) basis set on structures optimized with the 6-31G(d,p) basis set are indicated between parentheses

		IR	TS	P
Protonated	$\Delta E_{0,\varepsilon=1}$	0.0 (0.0)	169.7 (159.8)	−28.7 (−33.8)
	$\Delta E_{\varepsilon=1}$	0.0	162.9	−30.9
	$\Delta H_{\varepsilon=1}$	0.0	162.9	−30.9
	$\Delta G_{\varepsilon=1}$	0.0	166.0	−35.1
Deprotonated	$\Delta E_{0,\varepsilon=1}$	0.0 (0.0)	140.5 (127.3)	−33.4 (−39.0)
	$\Delta E_{\varepsilon=1}$	0.0	132.4	−34.9
	$\Delta H_{\varepsilon=1}$	0.0	132.4	−34.9
	$\Delta G_{\varepsilon=1}$	0.0	131.7	−37.5

oxetane ring opening starting earlier than the N–H bond breaking.

In a vacuum, the activation barrier associated with the elementary step is quite high, with an enthalpy of activation and a Gibbs energy of activation of 163 kJ mol^{-1} and 166 kJ mol^{-1} respectively for a protonated phosphate group. The activation barrier is slightly lowered in the case of a deprotonated phosphate group, with an enthalpy of activation of 132 kJ mol^{-1} and a Gibbs energy of activation of 132 kJ mol^{-1} too. Nonetheless, it remains very high.

Table 3 Evolution of the enthalpy H and Gibbs energy G (in kJ mol^{-1}) at T = 298 K and P = 1 atm during the IR–TS–P elementary step for protonated and deprotonated states of the phosphate group, in a vacuum (ε = 1) and in a water solvent modeled by PCM (ε = 78)

		IR	TS	P
Protonated	$\Delta H_{\varepsilon=78}$	0.0	136.4	−36.6
	$(\Delta H_{\varepsilon=1})$	(0.0)	(162.9)	(−30.9)
	$\Delta G_{\varepsilon=78}$	0.0	139.6	−40.9
	$(\Delta G_{\varepsilon=1})$	(0.0)	(166.0)	(−35.1)
Deprotonated	$\Delta H_{\varepsilon=78}$	0.0	121.7	−41.8
	$(\Delta H_{\varepsilon=1})$	(0.0)	(132.4)	(−34.9)
	$\Delta G_{\varepsilon=78}$	0.0	121.0	−44.4
	$(\Delta G_{\varepsilon=1})$	(0.0)	(131.7)	(−37.5)

As for the enthalpy of reaction and the Gibbs energy of reaction they are of −31 and −35 kJ mol^{-1} respectively in the case of the protonated phosphate group and of −35 and −38 kJ mol^{-1} respectively in the case of the deprotonated phosphate group. In other words, the elementary step appears slightly exergonic.

Note that the single point energy calculations performed on the stationary points with the same basis set augmented with diffuse functions show the same qualitative trend. Nonetheless, quantities of activation and reaction differ by about 5–10 kJ mol^{-1} from those obtained with the 6-31G(d,p) basis set, indicating that numeric values extracted from our computations have to be taken with caution.

4.1.2. Bulk effect of an aqueous environment. In biological systems, DNA is immersed in an aqueous environment, which is at the same time polar and protic. In order to evaluate in a first step the effect of polarity on the energetics of the IR–TS–P elementary step, single point energy calculations were performed on IR, TS and P placing them in a cavity surrounded by a polarized continuum characterized by a dielectric constant of ε = 78.39. The corresponding quantities of activation and reaction are reported in Table 3 where values obtained in a vacuum are also shown.

It appears that polarity of the environment tends to lower the activation barriers by about 25 kJ mol^{-1} when the phosphate group is protonated and by about 10 kJ mol^{-1} when it is deprotonated. In addition, the IR–TS–P elementary step appears to be slightly more exothermic/exergonic, with an enthalpy and a Gibbs energy of reaction more negative by about 6–8 kJ mol^{-1}, independently from the protonation state of the phosphate group. Thus, a polar environment facilitates the oxetane ring opening by intramolecular H transfer. Nonetheless, all in all, in a polar environment such as in a vacuum, it is characterized by a very high energy barrier and a rather weak driving force. Thus, the fact that experimentally the oxetane intermediate has never been isolated cannot be rationalized on the basis of these results. Thus another mechanism for the oxetane ring opening was considered, involving the participation of water molecules from the surroundings.

4.2. Assistance of water molecules

It is well established that the presence of a (6-4) photoproduct in double-stranded DNA induces large structural distortions,

much larger for example than those for a cyclobutane pyrimidine dimer.[27–29] The formation of the oxetane intermediate can be seen as a first step in the appearance of these distortions, which, at this point, must be comparable though slightly larger than those accompanying a CPD. As a result, few water molecules are likely to be present in the proximity of the oxetane ring. It thus seems reasonable that a water molecule (or a few) can participate in the H3′ proton transfer process which will then proceed in an indirect way.

We investigated the possibility that one and then two water molecules assist in the ring opening process. A transition state linking directly the oxetane intermediate (in interaction with one or two water molecules) and the 6-4PP product (in interaction with one or two water molecules) could be optimized in both cases. They are named hereafter TS-H_2O and TS-$2H_2O$ respectively.

With one assisting water molecule, during the step, H3′ is transferred from N3′ to the oxygen of the water molecule (O_w), a proton is transferred (H_w) from the water molecule to O4′ and the C4′–O4′ is broken. As such, the transition state structure can be described as a '6 centres transition state'. Structures of the corresponding reactant (IR-H_2O), transition state (TS-H_2O) and product (P-H_2O) in the case of a protonated phosphate group are shown in Fig. 4. Structures obtained in the case of a deprotonated phosphate group are very similar as can be inferred from the evolution of key distances affected during the step reported in Table 4.

In the TS-H_2O transition state structure, the N3′–H3′ bond is slightly more elongated (1.23 Å if the phosphate group is protonated; 1.13 Å if it is not) than it was in TS (1.06 Å if the phosphate group is protonated; 1.04 Å if it is not). As for the C4′–O4′ distance, it is 2.12 Å in TS-H_2O compared to 2.30 Å in TS when the phosphate group is protonated, and 2.39 Å in TS-H_2O compared to 2.33 Å in TS when the phosphate group is deprotonated. These modifications are quite small and it can then be concluded that the assistance of the water molecule does not affect significantly the synchronicity between the N3′–H3′ bond breaking and the oxetane ring opening.

Table 4 Evolution of key interatomic distances (in Å) during the IR-H_2O–TS-H_2O–P-H_2O elementary step for protonated and deprotonated states of the phosphate group

		IR-H_2O	TS-H_2O	P-H_2O
Protonated	$l_{N3'–H3'}$	1.02	1.23	2.65
	$l_{H3'–Ow}$	2.04	1.28	0.97
	$l_{Ow–Hw}$	0.97	1.10	1.84
	$l_{Hw–O4'}$	2.16	1.37	0.99
	$l_{C4'–O4'}$	1.47	2.12	2.71
Deprotonated	$l_{N3'–H3'}$	1.02	1.13	2.59
	$l_{H3'–Ow}$	2.24	1.44	0.97
	$l_{Ow–Hw}$	0.97	1.12	1.89
	$l_{Hw–O4'}$	2.07	1.34	0.98
	$l_{C4'–O4'}$	1.48	2.39	2.72

With two assisting water molecules, the elementary step consists of the H3′ transfer from N3′ to the oxygen (Ow1) of a first water molecule, transfer of one proton (Hw1) of this first water molecule to the oxygen (Ow2) of the second water molecule, transfer of one proton (Hw2) of this second water molecule to oxygen O4′ and breaking of the C4′–O4′ bond. Then, TS-$2H_2O$ is a '8 centres transition state'. Fig. 5 shows the optimized structures for the reactant (IR-$2H_2O$), transition state (TS-$2H_2O$) and product (P-$2H_2O$) of the step in the case of a protonated phosphate group. Once again, the corresponding structures in the case of a deprotonated phosphate group are very similar.

In Table 5 the distances affected during the step are reported. It can be noticed that in the case of a protonated phosphate group, at the transition state structure, the N3′–H3′ bond breaking is more advanced than in TS or even in TS-H_2O. Indeed, the N3′–H3′ distance is already 1.59 Å while it was 1.23 Å in TS-H_2O and 1.06 Å only in TS. In contrast, the C4′–O4′ bond breaking is less advanced with a C4′–O4′ separation

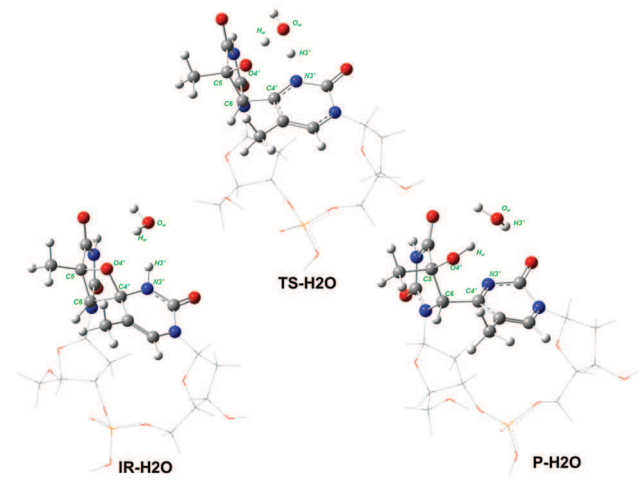

Fig. 4 Optimized geometries of IR-H_2O, TS-H_2O and P-H_2O in the case of a protonated phosphate group.

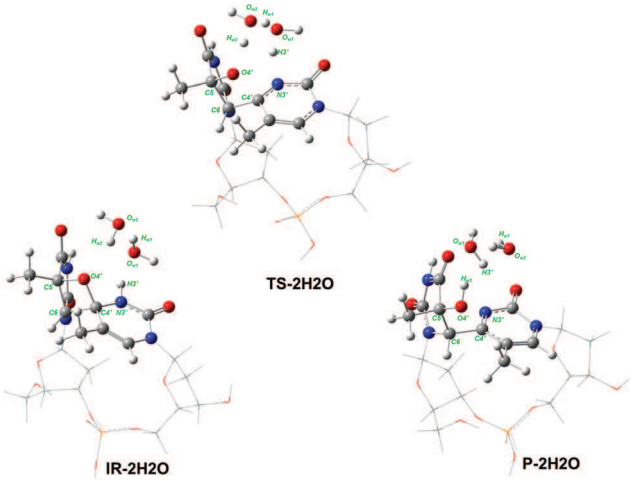

Fig. 5 Optimized geometries of IR-$2H_2O$, TS-$2H_2O$ and P-$2H_2O$ in the case of a protonated phosphate group.

Table 5 Evolution of key interatomic distances (in Å) during the IR-2H_2O–TS-2H_2O–P-2H_2O elementary step for protonated and deprotonated states of the phosphate group

		IR-2H_2O	TS-2H_2O	P-2H_2O
Protonated	$l_{N3'\text{-}H3'}$	1.04	1.59	2.61
	$l_{H3'\text{–}Ow1}$	1.79	1.04	0.98
	$l_{Ow1\text{–}Hw1}$	0.98	1.19	1.99
	$l_{Hw1\text{–}Ow2}$	1.83	1.24	0.97
	$l_{Ow2\text{–}Hw2}$	0.97	1.04	3.59
	$l_{Hw2\text{–}O4'}$	2.08	1.51	0.98
	$l_{C4'\text{–}O4'}$	1.48	1.84	2.84
Deprotonated	$l_{N3'\text{–}H3'}$	1.03	1.23	2.61
	$l_{H3'\text{–}Ow1}$	1.89	1.27	0.98
	$l_{Ow1\text{–}Hw1}$	0.98	1.11	1.99
	$l_{Hw1\text{–}Ow2}$	1.88	1.36	0.97
	$l_{Ow2\text{–}Hw2}$	0.97	1.12	3.59
	$l_{Hw2\text{–}O4'}$	2.03	1.34	0.98
	$l_{C4'\text{–}O4'}$	1.50	2.36	2.84

of 1.89 Å in TS-2H_2O, 2.12 Å in TS-H_2O and 2.30 Å in TS. Thus, with a protonated phosphate group, assisting water molecules tend to resynchronize the H3′ proton transfer and the oxetane ring opening, advancing the former process and delaying the latter one. This is not so obvious in the case of a deprotonated phosphate group, since in TS-2H_2O, the N3′–H3′ separation is 1.23 Å, quite close to what it is in TS-H_2O (1.13 Å) and TS (1.04 Å). As for the C4′–O4′ separation, it is 2.36 Å in TS-2H_2O, 2.39 Å in TS-H_2O and 2.33 Å in TS, *i.e.* almost identical.

The enthalpies and Gibbs energies of activation and reaction, in a polar environment, for the oxetane ring processes involving one and two assisting water molecules are reported in Table 6, together with those obtained in the case of oxetane ring opening *via* a direct intramolecular proton transfer. It appears quite clear that intervention of one water molecule from the solvent to induce the H3′ transfer and the oxetane ring opening considerably lowers the activation barrier. The enthalpies and Gibbs energies of activation are lowered by about 55–60 kJ mol^{-1} when one water molecule assists the ring opening process, whether the phosphate group is protonated or not. The intervention of a second water molecule increases this catalytic effect, but to a smaller extent since between one and two assisting molecules, the activation barrier is lowered by 10–20 kJ mol^{-1} depending on the protonation state of the phosphate group. From a kinetic perspective, the most favorable situation is that with a deprotonated phosphate group and two assisting water molecules. In that case, the Gibbs energy of activation is as low as +44 kJ mol^{-1}.

The overall energetics for the ring opening reaction remains relatively similar whether or not one water molecule assists. As soon as a second water molecule comes into play, it appears that the exergonicity of the ring opening process is increased in the case of the deprotonated phosphate group (by ~25 kJ mol^{-1}) while it remains globally the same for the protonated phosphate group. Therefore, from a thermodynamic perspective too, the most favorable situation is that with a deprotonated phosphate group and two assisting water molecules. Then the Gibbs energy of reaction is about −72 kJ mol^{-1}.

Therefore, in the hypothesis of an intermediate formed by the photochemical process leading to 6-4PP photoproducts, its decomposition needs the intervention of at least one water molecule from the solvent, and most probably two. The exergonicity of the reaction can help in explaining why the oxetane intermediate has not been experimentally isolated to date.

Table 6 Enthalpy of activation ($\Delta\Delta H^{\neq}_{\varepsilon=78}$), enthalpy of reaction ($\Delta\Delta H^{\circ}_{\varepsilon=78}$), Gibbs energy of activation ($\Delta\Delta G^{\neq}_{\varepsilon=78}$) and Gibbs energy of reaction ($\Delta\Delta G^{\circ}_{\varepsilon=78}$) of the oxetane ring opening elementary step at T = 298 K and P = 1 atm, in a water solvent modeled by PCM (ε = 78), without the assistance of any water molecule (IR–TS–P), and with the assistance of either one (IR-H_2O–TS-H_2O–P-H_2O) or two (IR-H_2O–TS-H_2O–P-H_2O) water molecules, for both protonated and deprotonated phosphate groups (in kJ mol^{-1})

		$0H_2O$	$1H_2O$	$2H_2O$
Protonated	$\Delta\Delta H^{\neq}_{\varepsilon=78}$	136.4	77.9	60.1
	$(\Delta\Delta H^{\circ}_{\varepsilon=78})$	(−36.6)	(−36.8)	(−33.0)
	$\Delta\Delta G^{\neq}_{\varepsilon=78}$	139.6	82.7	72.5
	$(\Delta\Delta G^{\circ}_{\varepsilon=78})$	(−40.9)	(−39.3)	(−33.3)
Deprotonated	$\Delta\Delta H^{\neq}_{\varepsilon=78}$	121.7	62.7	40.3
	$(\Delta\Delta H^{\circ}_{\varepsilon=78})$	(−41.8)	(−44.4)	(−69.8)
	$\Delta\Delta G^{\neq}_{\varepsilon=78}$	121.0	67.4	44.3
	$(\Delta\Delta G^{\circ}_{\varepsilon=78})$	(−44.4)	(−45.7)	(−72.0)

5. Conclusions

In this work, using a dinucleoside monophosphate as a model, we studied different reaction pathways for the formation of the thymine–thymine pyrimidine (6-4) pyrimidone from the corresponding oxetane. Their study *in silico* by DFT indicates that: (1) the oxetane corresponds to a local minimum on the ground state potential energy surface, indicating that it is electronically stable; (2) the oxetane ring opening process by intramolecular proton transfer is not feasible from a kinetic point of view, though slightly favored by the polar character of the aqueous environment; (3) if one or even better two water molecules from the environment participate in the reaction, opening of the 4-membered ring to form the (6-4) photoadduct is associated with an activation barrier low enough to explain the rapid clearance of the oxetane intermediate from the medium. Taken together, these findings bring further support to the idea according to which the generation of 6-4PPs proceeds *via* the formation of an oxetane intermediate.

It would be of interest in future work to evaluate more quantitatively the easiness to break the oxetane/azetidine intermediate at different bipyrimidic sites to determine to what extent it is involved in the difference of reactivity of thymine and cytosine observed regarding the formation of (6-4) photoproducts, which has been proposed to originate from differences in the electrophilic/nucleophilic character of the exocyclic O of thymine/N of cytosine in the excited state.

Acknowledgements

L. A. E. gratefully acknowledges funding from the Faculty of Science at the University of Gothenburg and the Swedish Science Research Council (VR).

Notes and references

1 V. O. Melnikova and H. N. Ananthaswamy, Cellular and molecular events leading to the development of skin cancer, *Mutat. Res.*, 2005, **571**, 91–106.
2 J. Cadet, E. Sage and T. Douki, Ultraviolet radiation-mediated damage to cellular DNA, *Mutat. Res.*, 2005, **571**, 3–17.
3 D. E. Brash, J. A. Rudolph, J. A. Simon, A. Lin, G. J. McKenna, H. P. Baden, A. J. Halperin and J. Ponten, A role for sunlight in skin cancer: UV-induced p53 mutations in squamous cell carcinoma, *Proc. Natl. Acad. Sci. U. S. A.*, 1991, **88**, 10124–10128.
4 N. Dumaz, C. Drougard, A. Sarasin and A. L. Daya-Grosjean, Specific UV-induced mutation spectrum in the p53 gene of skin tumors from DNA-repair-deficient xeroderma pigmentosum patients, *Proc. Natl. Acad. Sci. U. S. A.*, 1993, **90**, 10529–10533.
5 M. Charlier and C. Hélène, Photochemical reactions of aromatic ketones with nucleic acids and their components. I. Purine and pyrimidine bases and nucleosides, *Photochem. Photobiol.*, 1972, **15**, 71–87.
6 S. Encinas, N. Belmadoui, M. J. Climent, S. Gil and M. A. Miranda, Photosensitization of thymine nucleobase by benzophenone derivatives as models for photoinduced DNA damage: Paterno-Büchi *vs* energy and electron transfer processes, *Chem. Res. Toxicol.*, 2004, **17**, 857–862.
7 P. Clivio, J.-L. Fourrey and J. Gasche, DNA photodamage mechanistic studies: Characterization of a thietane intermediate in a model reaction relevant to "6-4 lesions", *J. Am. Chem. Soc.*, 1991, **113**, 5481–5483.
8 S. Marguet and D. Markovitsi, Time-resolved study of thymine dimer formation, *J. Am. Chem. Soc.*, 2005, **127**, 5780–5781.
9 M. Charlier and C. Hélène, Photosensitized dimerization of orotic acid in aqueous solution, *Photochem. Photobiol.*, 1967, **6**, 501–504.
10 R. Ben-Ishai, E. Ben-Hur and Y. Hornfeld, Photosensitized dimerization of thymine and cytosine in DNA, *Isr. J. Chem.*, 1968, **6**, 769–775.
11 T. Douki and J. Cadet, Far-UV photochemistry and photosensitization of 2′-deoxycytidylyl-(3′–5′)-thymidine: Isolation and characterization of the main photoproducts, *J. Photochem. Photobiol. B: Biol.*, 1992, **15**, 199–213.
12 T. Douki and J. Cadet, Individual determination of the yield of the main-UV induced dimeric pyrimidine photoproducts in DNA suggests a high mutagenicity of CC photolesions, *Biochemistry*, 2001, **40**, 2495–2501.
13 S. Courdavault, C. Baudouin, M. Charveron, B. Canghilem, A. Favier, J. Cadet and T. Douki, Repair of the three main types of bipyrimidine DNA photoproducts in human keratinocytes exposed to UVB and UVA radiations, *DNA Repair*, 2005, **4**, 836–844.
14 S. Mouret, C. Baudouin, M. Charveron, A. Favier, J. Cadet and T. Douki, Cyclobutane pyrimidine dimers are predominant DNA lesions in whole human skin exposed to UVA radiation, *Proc. Natl. Acad. Sci. U. S. A.*, 2006, **103**, 13765–13770.
15 T. Douki, A. Reynaud-Angelin, J. Cadet and E. Sage, Bipyrimidine photoproducts rather than oxidative lesions are the main type of DNA damage involved in the genotoxic effect of solar UVA radiation, *Biochemistry*, 2003, **42**, 9221–9226.
16 B. Durbeej and L. A. Eriksson, Reaction mechanism of thymine dimer formation in DNA induced by UV light, *J. Photochem. Photobiol. A: Chem.*, 2002, **152**, 95–101.
17 B. Durbeej and L. A. Eriksson, On the formation of cyclobutane pyrimidine dimers in UV-irradiated DNA: Why are thymines more reactive?, *Photochem. Photobiol.*, 2003, **78**, 159–167.
18 J. J. Serrano-Perez, I. Gonzalez-Ramirez, P. B. Coto, M. Merchan and L. Serrano-Andres, Theoretical insight into the intrinsic ultrafast formation of cyclobutane pyrimidine dimers in UV-irradiated DNA: Thymine versus cytosine, *J. Phys. Chem. B*, 2008, **112**, 14096–14098.
19 L. Blancafort and A. Migani, Modeling thymine photodimerizations in DNA: mechanism and correlation diagrams, *J. Am. Chem.Soc.*, 2007, **129**, 14540–14541.
20 A. Banyasz, T. Douki, R. Improta, T. Gustavsson, D. Onidas, I. Vaya, M. Perron and D. Markovitsi, Electronic excited states responsible for dimer formation upon UV absorption directly by thymine strands: Joint experimental and theoretical study, *J. Am. Chem. Soc.*, 2012, **134**, 14834–14845.
21 R. Improta, Photophysics and photochemistry of thymine deoxy-dinucleotide in water: A PCM/TD-DFT quantum mechanical study, *J. Phys. Chem. B*, 2012, **116**, 14261–14274.
22 C. Morell, V. Labet, P. W. Ayers, L. Genovese, A. Grand and H. Chermette, Use of the dual potential to rationalize the occurrence of some DNA lesions (pyrimidic dimers), *J. Phys. Chem. A*, 2011, **115**, 8032–8040.
23 (*a*) M. J. Frisch, *et al.*, *Gaussian 03 (Revisions C.02)*, Gaussian, Inc., Wallingford CT, U.S.A., 2004; (*b*) M. J. Frisch, *et al.*, *Gaussian 03 (Revisions D.02)*, Gaussian, Inc., Wallingford CT, U.S.A., 2006; (*c*) M. J. Frisch, *et al.*, *Gaussian 09 (Revisions A.02)*, Gaussian, Inc., Wallingford CT, U.S.A, 2009.
24 M. T. Cancès, B. Mennucci and J. Tomasi, A new integral formalism for the polarizable continuum model: Theoretical background and applications to isotropic and anisotropic dielectrics, *J. Chem. Phys.*, 1997, **107**, 3032–3041.
25 B. Mennucci and J. Tomasi, Continuum solvation models: A new approach to the problem of solute's charge distribution and cavity boundaries, *J. Chem. Phys.*, 1997, **106**, 5151–5158.

26 M. Cossi, G. Scalmani, N. Rega and V. Barone, New developments in the polarizable continuum model for quantum mechanical and classical calculations on molecules in solution, *J. Chem. Phys.*, 2002, **117**, 43–54.

27 J. Kemmink, R. Boelens, T. Koning, G. A. van der Marel, J. H. van Boom and R. Kaptein, ^{1}H NMR study of the exchangeable protons of the duplex d(GCGTTGCG). d(CGCAACGC) containing a thymine photodimer, *Nucleic Acids Res.*, 1987, **15**, 4645–4653.

28 J. K. Kim and B. S. Choi, The solution structure of DNA duplex-decamer containing the (6-4) photoproduct of thymidyl(3′→5′)thymidine by NMR and relaxation matrix refinement, *Eur. J. Biochem.*, 1995, **228**, 849–854.

29 J. H. Lee, G. S. Hwang and B. S. Choi, Solution structure of a DNA decamer duplex containing the stable 3′ T.G base pair of the pyrimidine(6-4)pyrimidine photoproduct [(6-4) adduct]: Implications for the highly specific 3′ T→C transition of the (6-4) adduct, *Proc. Natl. Acad. Sci. U. S. A.*, 1999, **96**, 6632–6636.

